

Theory and measurement of bidirectional reflectance for signature analysis

James Jafolla^a, David Thomas^b, John Hilgers^c, Bill Reynolds^c, and Chris Blasband^a

^aSurface Optics Corporation, San Diego, CA 92127

^bU.S. Tank-Automotive and Armaments Command, Warren, MI 48397

^cSignature Research, Inc., Calumet, MI 49913

ABSTRACT

The application of advanced low observable treatments to ground vehicles has led to a requirement for a better understanding of effects of light scattering from surfaces. Measurements of the Bidirectional Reflectance Distribution Function (BRDF) fully describe the angular scattering properties of materials, and these may be used in signature simulations to quantitatively characterize the optical effects of surface treatments on targets. This paper reviews the theoretical and experimental techniques for characterizing the BRDF of surfaces and examines some of the popular parameterized BRDF representations that are used in signature calculations.

1.0 INTRODUCTION

The application of BRDF data in signature analysis to obtain visually realistic images and radiometric accuracy for system effectiveness evaluation is an ongoing issue for the modeling and simulation community. Most commercial visualization implementations use a simple specular/diffuse approximation to the surface optical properties. Even the more sophisticated signature analysis codes often resort to simplified, parameterized representations of the actual BRDF. The introduction of BRDF data into signature analysis raises a number of technical questions. How much BRDF data is required, and what is the necessary spectral and angular resolution? What requirements does this impose on the geometry model? What is the best way of representing BRDF data for accurate signature calculations? We will attempt to answer some of these questions by comparing BRDF measurements to parameterized representations of the BRDF.

2.0 BRDF DEFINITION

The function used to describe the directional dependence of the reflected energy from a surface is the Bidirectional Reflectance Distribution Function (BRDF). The geometry of the BRDF definition is shown in Figure 1

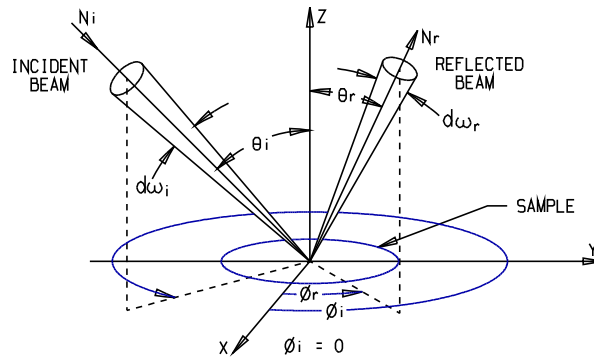


Figure 1 BRDF Geometry.

The BRDF is defined as the ratio of the reflected radiance ($w\text{-m}^{-2}\text{-sr}^{-1}$) in a particular direction (θ_r, ϕ_r) to the incident irradiance ($w\text{-m}^{-2}$) from direction (θ_i, ϕ_i) .

$$\rho'(\theta_i, \phi_i, \theta_r, \phi_r) = \frac{\delta N_r(\theta_r, \phi_r)}{N_i(\theta_i, \phi_i) \cos \theta_i \delta \omega_i} \quad (1)$$

The units of the BRDF are inverse solid-angle (sr^{-1}).

Figure 2, taken from the well-known paper by Nicodemus¹, shows a pictorial representation of a typical BRDF that provides a good physical description of these concepts.

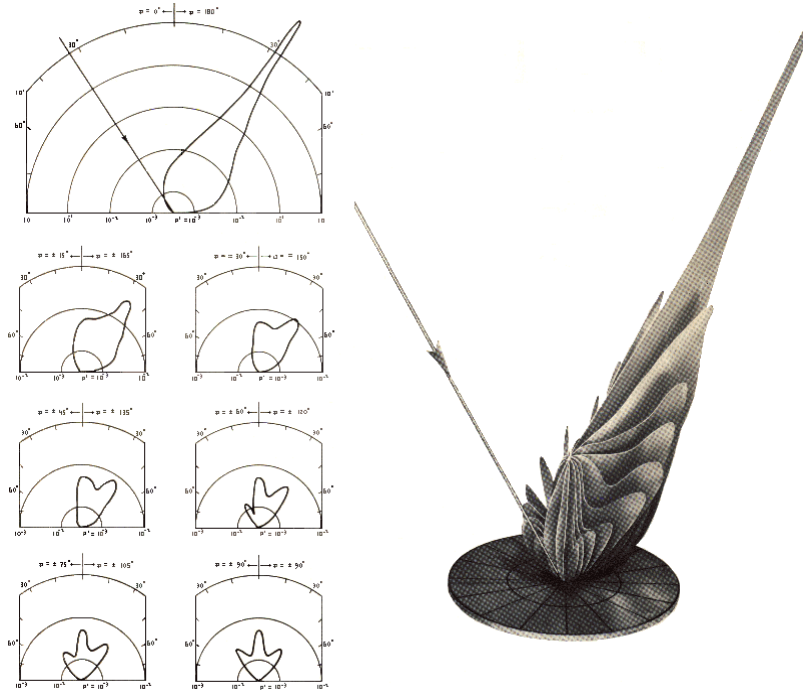


Figure 2 BRDF Visualization from Nicodemus¹.

The integral of the BRDF over all reflected angles provides the dimensionless Directional Hemispherical Reflectance (DHR). Similarly, the integral of the BRDF over all incident angles gives the Hemispherical Directional Reflectance (HDR). The BRDF is invariant under interchange of incident and reflected angles (reciprocity), therefore the HDR and DHR are equivalent, and can be used interchangeably.

3.0 BRDF PHENOMENOLOGY

The phenomenology of light scattering from surfaces involves a complex interaction between molecular scale phenomena, *e.g.*, electronic absorption, molecular and lattice vibrations, and macroscopic scale multiple scattering from particles and rough surfaces. For homogeneous materials with a RMS surface roughness much smaller than the wavelength of interest, the simplest representation of the BRDF is essentially a delta function whose magnitude is given by the Fresnel reflection formulas for oblique incidence.

$$\rho'(\theta_i, \phi_i, \theta_r, \phi_r) = \frac{\delta(\theta_r - \theta_i)\delta(\phi_r - \phi_i)}{2\pi \sin\theta_r} \frac{1}{2}(R_p + R_s) \quad (2)$$

where

$$R_p = \left| \frac{\cos\theta_t - m \cos\theta_i}{\cos\theta_t + m \cos\theta_i} \right|^2 \quad (3)$$

$$R_s = \left| \frac{\cos\theta_i - m \cos\theta_t}{\cos\theta_i + m \cos\theta_t} \right|^2$$

and R_p and R_s are the ratio of the incident to reflected irradiances for parallel and perpendicular polarized light, θ_i and θ_r are the incident and transmitted angles and m is the complex refractive index of the medium. When the surface roughness is comparable or larger than the wavelength and/or the medium is non-homogeneous, light interactions with the surface become considerably more complex. In this case rough surface scattering and single and multiple scattering from embedded particles affect the BRDF of the surface. Figure 3 shows a schematic depiction of the phenomenology of light reflecting from a paint surface.

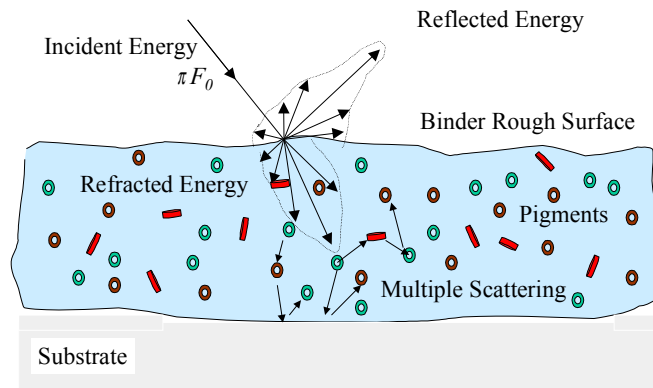


Figure 3 Schematic depiction of light interacting with a paint surface.

Understanding the generalized light scattering from surfaces is still very much an active area of research, and is a topic of numerous international workshops and symposia, *e.g.*, Gu and Maradudin². One approach to describing the BRDF of complex surfaces such as paints is to calculate the surface and volume scattering contributions separately, using rough surface scattering analysis and single and multiple scattering from pigments, and then to radiatively couple the two effects using the Adding/Doubling radiative transfer technique. Jafolla, Sullivan and Stokes³ discussed this engineering analysis of the BRDF of paint surfaces in a recent paper.

4.0 BRDF MEASUREMENTS

Accurate BRDF measurements for signature analysis requires a systematic mapping of the light scattered in the hemisphere. A paper by Thomas, *et al*⁴ describes the laboratory and field Bi-Directional Reflectometers (BDR) at TACOM and CDNSWC that are used to perform these measurements for signature analysis applications. Figure 4 shows the in-situ BRDF system in use at TACOM for performing laboratory and field measurements and Figure 5 shows the laboratory instrument at CDNSWC.

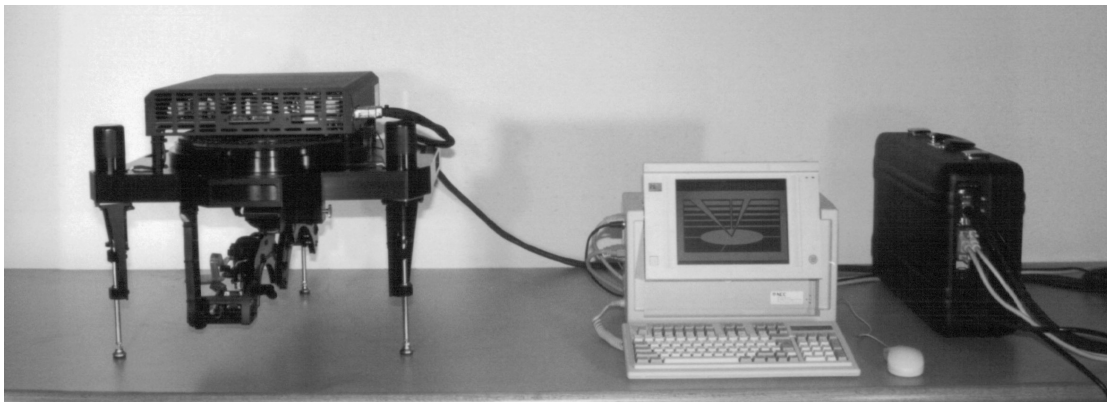


Figure 4 SOC-250 In-Situ Bidirectional Reflectometer.



Figure 5 SOC-200 Laboratory Bidirectional Reflectometer.

The SOC-200 is a fully automated instrument provides full hemispheric coverage for both unpolarized BRDF and Mueller matrix measurements. Light sources for the measurements include quartz halogen and 1700°C blackbody broadband sources, and up to five optional laser sources. A number of detectors are employed, e.g., photomultiplier tube, lead sulfide, mercury cadmium telluride, to provide continuous spectral coverage from 0.3 to 14 microns. Wavelength selection is accomplished by inserting thin film bandpass filters into the optical train in front of the detectors. The noise floor of the instrument is 10^{-3} ster⁻¹ for broadband sources and 10^{-6} ster⁻¹ for laser sources. A paper by Beecroft, *et al*⁵ provides a detailed description of the capabilities of this instrument. Figure 6 shows a three dimensional plot of the BRDF of Army Green 383 at a wavelength of 0.5 microns and 50° incident angle.

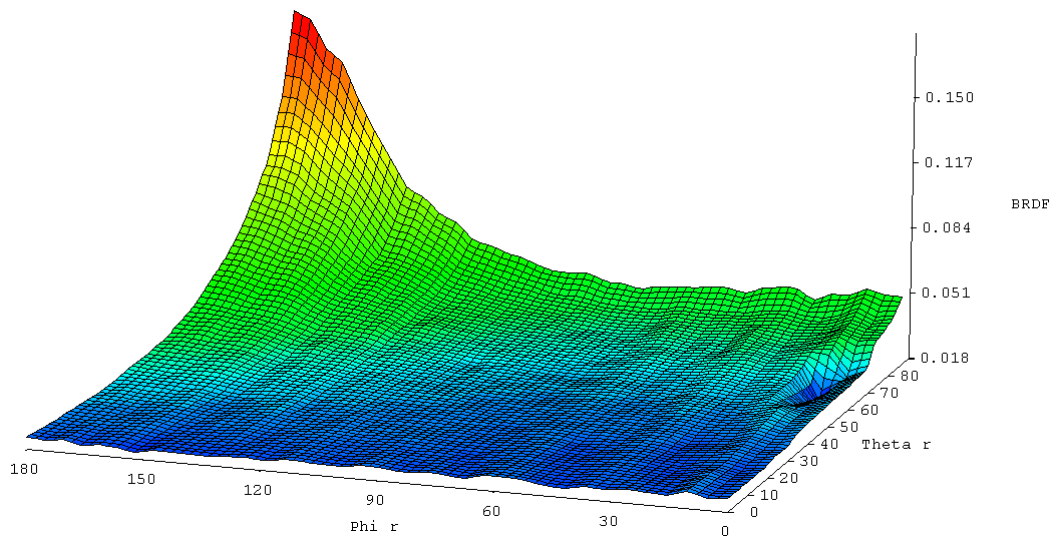


Figure 6 BRDF of Army Green 383 at 0.5 Microns and 50° Incident Angle.

4.1 Imaging Bidirectional Reflectometers

The instrumentation described above are referred to as goniometers, because positioning the source and detector along the goniometric coordinates above the sample performs the measurement. Recently, Boeing Defense and Space Group and Surface Optics Corporation, under contract from the Air Force Research Laboratory, have developed a new hand-held instrument⁶, shown in Figure 7, capable of simultaneously measuring both BRDF and HDR of a surface in-situ. Using a patented angular imaging technique and a micro-bolometer array, the instrument fully maps the scattering from a half-hemisphere above the surface with more than 30,000 angularly resolved points and update rates to 60 measurements per second. The instrument then computes HDR from the measured BDR. Beam incidence elevation is variable from, $\theta_i = 0^\circ$ to 85° , while scattering is measured to nearly 90° off normal.



Figure 7 Hand-Held imaging HDR-BRDF instrument.

Each pixel in the “angular image” formed on the array corresponds to a small range of scattering angles relative to the illuminated spot on the measured surface, as shown in Figure 8. If the detector response is known for each pixel, the images may be interpreted as a quantitative measurement of the angular distribution of the reflected light. Alternatively, dividing by the incident intensity of the illuminating beam, the image can be interpreted as revealing the angular distribution of reflectance from the sample. Summing over the image determines the total reflectance, though this is complicated by the fact that not all scattered rays are captured in the image.

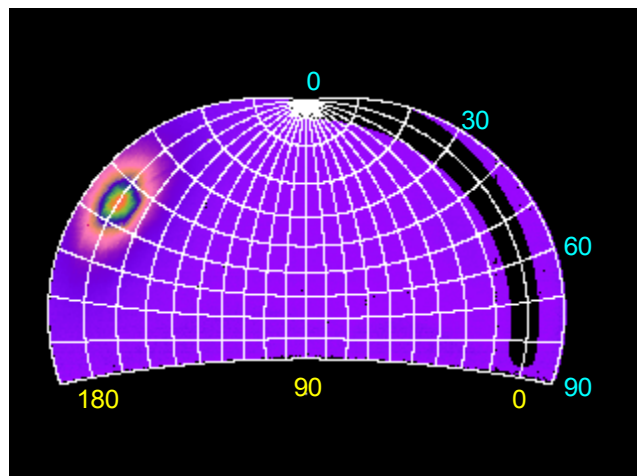


Figure 8 Angle image formed by the HHDR showing 3-5 μm reflected light distribution for an incidence angle of 45° .

4.2 Mueller Matrix Measurements

Another important issue for signature analysis is the determination of polarization features of targets and backgrounds. The Stokes vector is most often used to describe the generalized representation of partially polarized light. The transformation of the incident to reflected Stokes vector is specified by the Mueller Matrix of the surface. Mueller matrix measurements can be made at wavelengths in the 0.3 to 14.0 μm band, subject to laser availability. Waveplates are necessarily tuned to the laser wavelength employed. Polarizers may be obtained to function at more than one wavelength, but not all wavelengths.

Light in an arbitrary polarization state reflected, scattered or transmitted from a two dimensional sample surface can be related to the polarization state of the incident light by a square matrix of 16 elements (4x4). This matrix, called the Mueller matrix, completely characterizes the interaction of the sample with the incident radiation. It is a function of wavelength and in the case of scattering is a function of all four angles defining the incident and reflected radiation. It is a necessary part of the complete optical description of scattering measurements made with a coherent source.

The schematic measurement setup, which permits determination of the Mueller matrix, is shown in Figure 9. The input optics can be set to produce unpolarized radiation (circularly distributed amplitude of the electric vector with random phase). This is achieved by continuous stepwise rotation of both the half waveplate and the quarter waveplate as shown on the laser side. This method permits development of statistical data averaged over all positions of the plates with a high signal-to-noise ratio for poorly reflecting surfaces. By setting the $\lambda/2$ plate to 45° the experimenter can illuminate with horizontally polarized radiation. By rotating the $\lambda/2$ plate $+22.5^\circ$, the incident radiation can be set to 45° away from the vertical reference axis. Finally by setting the $\lambda/2$ plate to zero and rotating the $\lambda/4$ plate $+45^\circ$ the condition of the incident radiation can be set to right circular polarization.

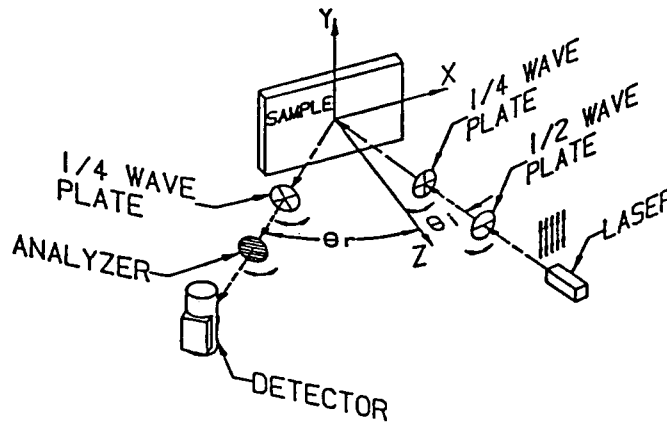


Figure 9. Schematic measurement setup for Mueller matrix evaluation.

The polarization characteristics of the incident and reflected light are represented by four-element vector, called the Stokes vector. The incident Stokes vector can now be represented by a column matrix, given by

$$[I] = \begin{bmatrix} [o] \\ [h] \\ [+] \\ [r] \end{bmatrix}, \quad \begin{matrix} o = \langle A_x^2 + A_y^2 \rangle \\ h = \langle A_x^2 - A_y^2 \rangle \\ + = \langle 2A_x A_y \cos \gamma \rangle \\ r = \langle 2A_x A_y \sin \gamma \rangle \end{matrix} \quad (4)$$

where A_x , A_y are amplitudes of the electric field vector, γ is the phase angle between A_x and A_y and $\langle \rangle$ indicates a time averaged quantity.

The four forms of incident radiation commonly used, expressed in row matrix form are:

- [1, 0, 0, 0]: *unpolarized radiation of unit intensity*
- [1, ± 1 , 0, 0]: *vertical (+) or horizontal (-) polarized radiation of unit intensity*
- [1, 0, ± 1 , 0]: *radiation of unit intensity polarized linearly at $\pm 45^\circ$ to the reference axis*
- [1, 0, 0, ± 1]: *right (+) or left (-) circularly polarized radiation of unit intensity*

The scattered Stokes vector (S) can be found from

$$\begin{matrix} (4 \times 1) \\ [S] \end{matrix} = \begin{matrix} (4 \times 4) \\ \begin{bmatrix} M_{11} & M_{12} & M_{13} & M_{14} \\ M_{21} & M_{22} & M_{23} & M_{24} \\ M_{31} & M_{32} & M_{33} & M_{34} \\ M_{41} & M_{42} & M_{43} & M_{44} \end{bmatrix} \end{matrix} \cdot \begin{matrix} (4 \times 1) \\ [I] \end{matrix}, \quad (5)$$

In this equation [M] is the Mueller matrix and [S] is the scattered Stokes vector, without the modifications made to it by the optical components on the detector side (Figure 9). On the detector side of the sample the scattered Stokes vector is modified by combinations of 1/4 waveplate and analyzer settings designed to detect under various conditions of polarization. These exit Stokes vectors [E] are comparable to the incident vectors [I]. The usual set of E vectors expressed in row matrix form is:

- [1, 0, 0, 0]: *Unpolarized Detection*
- [1, ± 1 , 0, 0]: *Horizontal or Vertical Detection*
- [1, 0, ± 1 , 0]: *± 45 Degree Detection*
- [1, 0, 0, ± 1]: *Right or Left Circular Detection*

By setting the optical components for all combinations of incident and exit polarizations and recording the signals at the detector, the SOC-200 automatically produces a measurement matrix [P]:

$$[P] = \begin{bmatrix} P_{11} & P_{12} & P_{13} & P_{14} \\ P_{21} & P_{22} & P_{23} & P_{24} \\ P_{31} & P_{32} & P_{33} & P_{34} \\ P_{41} & P_{42} & P_{43} & P_{44} \end{bmatrix}, \quad (6)$$

The relation of each element of the [P] matrix to the Mueller matrix is then given by

$$P_{ij} = \begin{matrix} (1 \times 4) & (4 \times 4) & (4 \times 1) \\ [E] & [M] & [I] \end{matrix}. \quad (7)$$

Figure 10 shows some of the Mueller matrix elements of Army Green 383 measured at 0.5 microns and 20° incidence.

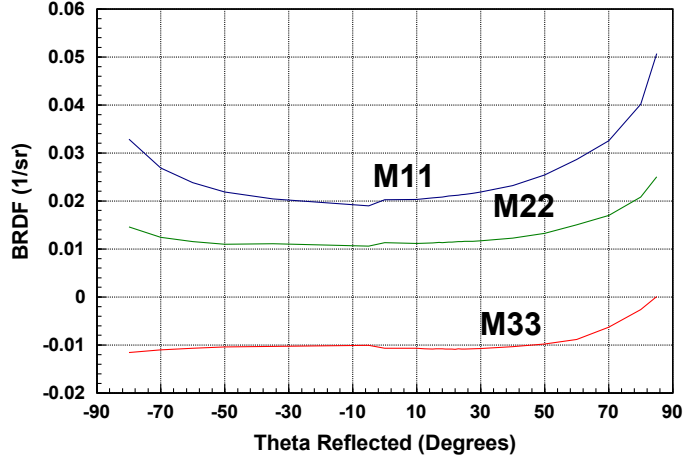


Figure 10 Mueller matrix measurements of Army Green 383 at 0.5 microns and 20° incidence

5.0 PARAMETERIZED BRDF MODELS

Signature analysis of realistic targets and backgrounds typically specifies a wide variety of materials in the scene. Also, a full spatial and spectral characterization of the BRDF requires a significant data collection effort, and produces a large volume of data. In order to manage the optical database and simplify the computational requirements, a number of parameterized representations of the BRDF have been developed. In this section, we will describe some of the parameterized BRDF models that are widely used in signature analysis: the Sandford-Robertson⁷ four-parameter model, the OPTASM Lorentzian lobe model developed by Acquista and Rosenwald⁸, and a newly developed Gaussian lobe model for representing the BRDF of complex surface structures.

5.1 Sandford-Robertson BRDF model

The Sandford-Robertson (SR) model is based on the assumption that the angular properties of the BRDF vary slowly with wavelength and can be separated from the spectral characteristics.

$$\rho'(\hat{k}_i, \hat{k}_r; \lambda) = f_r(\hat{k}_i, \hat{k}_r) \rho(\lambda) \quad (8)$$

where \hat{k}_i is the unit vector to the light source, \hat{k}_r is the unit vector to the receiver, and $\rho(\lambda)$ is the total spectral reflectance of the surface. It is further assumed the the angular dependence can be separated into a specular and diffuse component.

$$f_r(\hat{k}_i, \hat{k}_r) = f_D(\hat{k}_i, \hat{k}_r) + f_S(\hat{k}_i, \hat{k}_r) \quad (9)$$

The directional and spectral dependence of the emissivity is used to determine the diffuse scattering parameters, $\epsilon(\lambda)$ and b , from spectral HDR measurements

$$\begin{aligned} 1 - \rho(\theta, \lambda) &= \epsilon(\theta, \lambda) \\ &= \epsilon(\lambda) g(\theta) / G(b) \end{aligned} \quad (10)$$

where $\epsilon(\lambda)$ is the total spectral emissivity. The grazing angle dependence is given by

$$g(\theta) = 1 / (1 + b^2 \tan^2 \theta) \quad (11)$$

and the normalization constant of the angular distribution is

$$G(b) = \frac{1}{1-b^2} \left[1 - \frac{b^2}{1-b^2} \log(1/b^2) \right] \quad (12)$$

The diffuse component of the BRDF is given by

$$f_D(\hat{k}_i, \hat{k}_r) = \frac{1}{\pi} g(\theta_r) \rho_D(\lambda) g(\theta_i) / G^2(b) \quad (13)$$

The specular component of the BRDF lobe is assumed to be a circular ellipsoid centered on the specular angle with eccentricity e , defined by

$$f_S(\hat{k}_i, \hat{k}_r) = \frac{1}{4\pi} \rho_S(\theta_i, \lambda) \frac{h(\alpha)}{H(\theta_i) \cos \theta_r} \quad (14)$$

where

$$h(\alpha) = \frac{1}{(e^2 \cos^2 \alpha + \sin^2 \alpha)^2} \quad (15)$$

with α being the angle between the glint vector and the surface normal

$$\begin{aligned} \hat{g} &= (\hat{k}_r - \hat{k}_i) / \sqrt{2(1 - \hat{k}_i \cdot \hat{k}_r)} \\ \cos \alpha &= \hat{g} \cdot \hat{n} \end{aligned} \quad (16)$$

and the normalization factor being

$$H(\theta_i) = \frac{1}{2e^2} \left[(1 - e^2) \cos \theta + \frac{2e^2 + (1 - e^2)^2 \cos^2 \theta}{(1 - e^2)^2 \cos^2 \theta + 4e^2} \right] \quad (17)$$

Thus, the four SR model parameters are:

$$\begin{aligned} \rho_D(\lambda) &= \text{diffuse spectral reflectance} \\ \varepsilon(\lambda) &= \text{spectral emissivity} \\ b &= \text{grazing angle reflectivity} \\ e &= \text{width of specular lobe} \end{aligned}$$

with an additional constraint for defining the energy in the specular lobe

$$\rho_S(\lambda) = G(b) - \rho_D(\lambda) - \varepsilon(\lambda) \quad (18)$$

The SR model fitting procedure involves fitting the $\varepsilon(\lambda)$ and b parameters to the spectral HDR measurements. The b parameter is obtained from equation (4) by averaging the ratio of the near normal measurement to the measurements from 50 to 80 degrees. The $\rho_D(\lambda)$ and e parameters are obtained by iteratively adjusting the energy in the specular lobe and the shape so that a reasonable fit is achieved for each of the three incident angles (20, 40 and 60 degrees). The results of the SR model fit to the Army Green 383 measurements at 0.5 microns are shown in Figure 11.

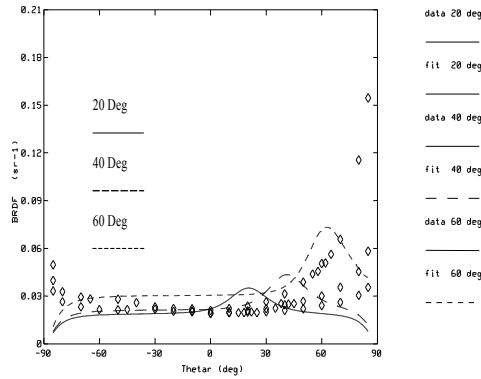


Figure 11 SR BRDF Fit to Army Green 383 at 0.5 Microns.

The SR model results do not show very good agreement with the data. Since the fitting process involves human judgement on what defines a “good fit” other analysts would produce different fits to the data. Our criteria was to choose SR parameters that qualitatively look the best for all three incident angles. A better approach would be to obtain the best fit for a specific input angle, e.g., 40°, which has the most impact on the signatures because of the solid angle weighting.

Another factor is that the analytic form of the SR model is simply not well suited to very diffuse paint systems. The grazing angle scattering that is characteristic of this type of coating cannot be modeled by a circular ellipsoid lobe fixed at the specular direction.

5.2 OPTASM BRDF model

The OPTASM BRDF model takes a somewhat more general approach to representing the BRDF in that the angular characteristics are specified by a number of Lorentzian shaped peaks. This provides flexibility in representing non-isotropic surfaces, which have peaks of scattered energy in non-specular directions. Typically, the BRDF is represented by two peaks, each defined by three parameters: the peak strength, A , the peak width in degrees, B , and the peak direction, \hat{k}_p , plus a constant term, ρ_o . (For isotropic materials, the ϕ_r location of the peak is assumed to be 180° from ϕ_i .) Thus, the BRDF is given by

$$\rho'(\hat{k}_i, \hat{k}_r) = \rho_o + A_1 / \{B_1^2 + 1 - \cos\Gamma_1\} + A_2 / \{B_2^2 + 1 - \cos\Gamma_2\} \quad (19)$$

where, $\Gamma = \cos^{-1}(\hat{k}_p \cdot \hat{k}_r)$, is the angle between the peak direction and the viewed direction.

One of the terms in this equation is used to represent the diffuse characteristic of the BRDF at grazing angles (similar to the SR b parameter) and the other term represents the main scattering lobe (similar to the SR e parameter) resulting in a seven parameter fit to the data. The parameters are fit to in-plane BRDF measurements using a Levenberg-Marquardt non-linear least-squares algorithm, and the peak strength parameters are then normalized to separate HDR measurements.

The flexibility of the OPTASM BRDF model lies in the fact that additional sets of parameters can be defined to represent more complicated scattering phenomenology. For example, many surfaces exhibit a distinct backscattering lobe and a bifurcation/shift of the forward scattering lobe from the specular direction for grazing incidence. Including additional Lorentzian lobes to the fitting function can represent these features.

The OPTASM BRDF model parameters are fit to the in-plane BRDF measurements at each incident angle and wavelength measured. The BRDF at other wavelengths and incident angles is obtained by interpolating over the parameter set. The HDR measurements for each incident angle and wavelength were then used to renormalize the strength parameters. The fitting procedure iteratively calls a Levenberg-Marquardt non-linear least squares fitting algorithm to adjust the parameters. The analyst monitors the chi-squared (goodness-of-fit) parameter and the graphic BRDF display until a satisfactory fit is obtained.

The results of fitting the OPTASM BRDF model to the measurements of Army Green 383 at 0.5 microns are shown in Figure 12. The fit for the OPTASM BRDF model appears much better than the SR model, particularly in capturing the grazing angle dependence for high incident angles. However, because the model parameters were fit at each incident angle, the comparison is between a 21-parameter model OPTASM model and a 4-parameter SR model.

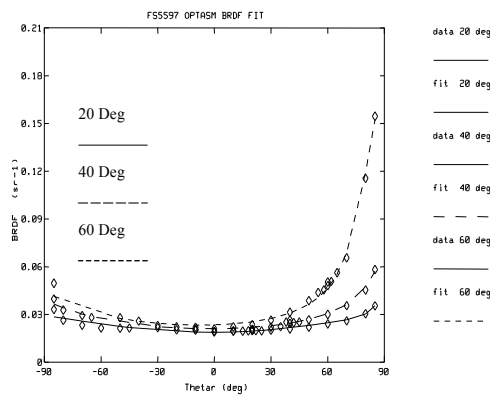


Figure 12 OPTASM BRDF Fit to Army Green 383 at 0.5 Microns.

5.3 Hilgers BRDF model

In applications requiring the BRDF for large numbers of (\hat{k}_i, \hat{k}_r) , for example, when integrating over large solid angles or in rendering for the production of physically accurate images, it is helpful to develop a model of the database which rapidly computes $\rho(\hat{k}_i, \hat{k}_r)$ with data files of manageable size.

The methodology of choice for accomplishing this depends on the degree to which rapidly varying lobes are present. If the surface is diffuse, so the BRDF is slowly varying, a coarse sampling grid may be used for all four angles. This results in a database of manageable size that can be directly interpolated.

However, if lobes of small angular subtense are present, the above procedure results in unreasonably large data files. For example, sampling all four angles at one-degree increments, which may well be required if specular features are present, results in about 10^9 floats. In this case, a “tracking” procedure is utilized. The tracking program operates in several modes. If the programmed angular increment in θ_i or ϕ_i loses contact with the lobe, a smaller increment, which may drop to one degree, is tried until the lobe is reacquired. If this fails, the user runs another utility to determine if the lobe truly vanished, and if so, where it reappears. This process constitutes the most difficult, time consuming and least automatic aspect of the entire project.

As flexible as the OPTASM model is in matching certain lobe structures, it has a disadvantage when applied to large databases involving large numbers of (\hat{k}_i, \hat{k}_r) . The seven OPTASM parameters are matched to the lobe data by the

non-linear, least squares Levenberg-Marquardt method. This method is very effective in single instances, but convergence is slow, requiring many iterations. Furthermore it is difficult to program an automatic method that will determine the minimal number of iterations necessary to guarantee sufficient accuracy for numerous incoming directions.

To remedy this problem, a model was sought which can be fit to the data by performing computations in the “forward direction”. This means a single calculation is performed on the data, which results in the determination of the model parameters, thus obviating the necessity of executing many iterations of a successive approximation technique.

Though a number of different such models were examined, the Gaussian model,

$$\rho'(\hat{k}_i, \hat{k}_r) = A e^{-\tau} \quad (20)$$

where

$$\tau = a(\theta_r - \bar{\theta}_r)^2 + 2b(\theta_r - \bar{\theta}_r)(\phi_r - \bar{\phi}_r) + c(\phi_r - \bar{\phi}_r)^2, \quad (21)$$

has the advantage of possessing finite second moments,

$$\begin{aligned} \mu_{xx} &= \iint x^2 e^{-\tau} dx dy = \pi c / d, \\ \mu_{yy} &= \iint y^2 e^{-\tau} dx dy = \pi a / d, \\ \mu_{xy} &= \iint xy e^{-\tau} dx dy = -\pi b / d, \end{aligned} \quad (22)$$

where

$$d = 2(ac - b^2)^{3/2}. \quad (23)$$

To use this model, all moments of the BRDF data up to the second are computed and equated to the corresponding Gaussian moment. The first moments determine $\bar{\theta}_r$ and $\bar{\phi}_r$. The lobe maximum determines A. The second moments determine a, b and c via,

$$\begin{aligned} a &= \mu_{yy} \mu_{\circ} / d \\ b &= -\mu_{xy} \mu_{\circ} / d \\ c &= \mu_{xx} \mu_{\circ} / d \end{aligned} \quad (24)$$

where this time,

$$d = 2(\mu_{xx}\mu_{yy} - \mu_{xy}^2) \quad (25)$$

and

$$\mu_{\circ} = \iint e^{-\tau} dx dy = \pi / \sqrt{ac - b^2} \quad (26)$$

is the zeroth moment.

As stated above, for each incoming direction, the position of all lobes is “tracked”, and the above calculations performed to determine the six model parameters: $A, \bar{\theta}_r, \bar{\phi}_r, a, b, c$ as functions of (θ_i, ϕ_i) . When the four angles are input to the model, this secondary database is interpolated with (θ_i, ϕ_i) to get the six parameters, and

these, with (θ_r, ϕ_r) in the Gaussian, yield the BRDF. While the same approach could be tried with the OPTASM model, no closed form expressions for the moments are known. Figure 13 shows a multi-lobed the BRDF from a pyramidal structured surface as computed by Surface Optics' MicroOpt program and the corresponding Gaussian model approximations.

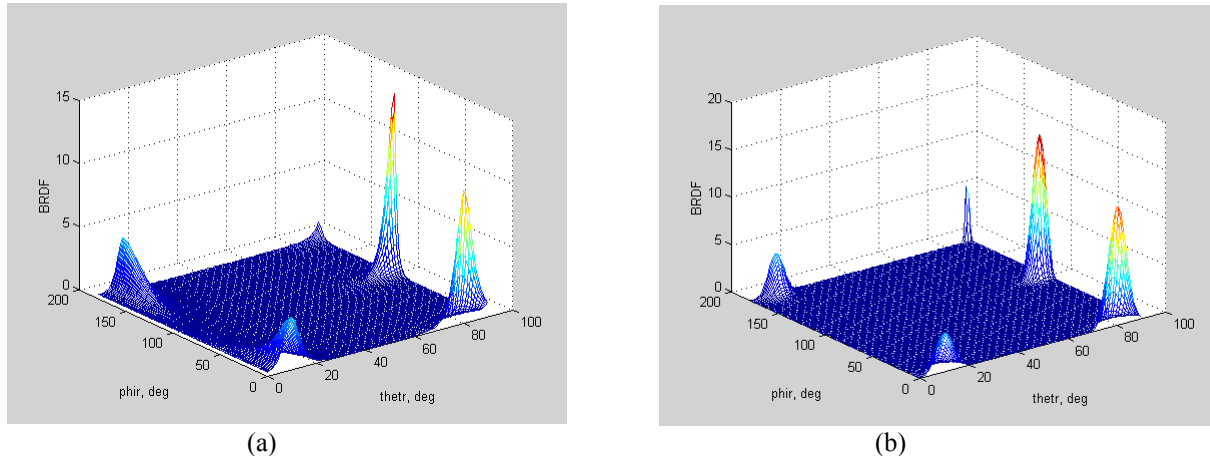


Figure 13. (a) MicroOpt and (b) Gaussian model for $\theta_i = 10$ and $\phi_i = 0$.

6.0 CONCLUSIONS

The ability to evaluate the effect of surface BRDF on signatures is becoming increasingly more important because of the ongoing development and application of LO surface treatments. The availability of automated bidirectional reflectometer instruments readily provides the BRDF measurement data, and it is clearly of interest to develop BRDF representations to exploit this data for signature analysis. Because of the complex phenomenology of light interactions with surfaces, parameterized models do not easily represent even the fairly simple case of a diffuse paint coating. Thus, it is clear that more work needs to be done in developing and validating BRDF model parameterizations if they are to be used for quantitative evaluation of surface treatments.

The results of this study suggest that the widely used Sandford-Robertson model is not the best choice for representing the BRDF of very diffuse paint systems. The assumptions of the analytic form of the specular lobe and the grazing angle reflectivity are not well suited to model the complex multiple scattering phenomenology that is characteristic of diffusely scattering surfaces.

The OPTASM BRDF model also has difficulty with very diffuse coatings that exhibit significant grazing angle scattering. The Lorentzian lobe parameters do a reasonable job fitting the measured data, but non-physical (i.e., negative) model parameters that can occur for very diffuse coatings show poor results when they are interpolated/extrapolated to other incident angles. A more constrained fitting procedure might help to alleviate this problem.

In general, the OPTASM BRDF model is much more flexible because the number and shape of the Lorentzian lobe parameters can be adjusted to fit both diffuse and specular scattering. Also, the direction of the scattering lobes are not constrained to be at the specular position which is better for representing the grazing angle gloss feature observed in many paint systems, as well as the small forward shift of the specular peak sometimes observed for moderately specular coatings. However, the large number of parameters required for accurate representation of the measured data (nominally, 21 parameters for the case presented here) negate some of the advantages of going to a simplified BRDF model in the first place.

ACKNOWLEDGEMENTS

The authors would like to thank Jim Crosby of TACOM for assistance in making the BRDF measurements.

REFERENCES

1. F. Nicodemus, "Directional Reflectance and Emissivity of an Opaque Surface", *Appl. Opt.*, **4**, pp. 767-773 (1965).
2. Z. Gu and A. Maridudin, eds., *Scattering and Surface Roughness II*, SPIE **Vol. 3426**, San Diego, (1998).
3. J. Jafolla, R. Sullivan and J. Stokes, "Phenomenological BRDF modeling for engineering applications," *Proceedings of the SPIE Symposium on Surface Scattering* San Diego, **Vol. 3141**, 281-292 (1997)
4. D. Thomas, J. Jafolla and P. Sarman, "Bidirectional Reflectance Measurements for High Resolution Signature Modeling," *Proceedings of the SPIE Symposium on Targets and Backgrounds: Characterization and Representation III*, Orlando, **Vol. 3062**, 105-116 (1997).
5. M. Beecroft, J. Neu and J. Jafolla, "Bidirectional reflectance data to support paint development and signature calculations," *Proceedings of the SPIE Symposium on Stray Radiation in Optical Systems II*, San Diego, **Vol. 1753**, 304-316 (1992).
6. P. Mattison, M Dombrowski, J. Lorenz, K. Davis, H. Mann, P. Johnson and B. Foos, "The Hand-Held Directional Reflectometer: An angular imaging instrument to measure BRDF and HDR in real time," *Scattering and Surface Roughness II*, SPIE **Vol. 3426**, 240-251, (1998).
7. B. Sandford and D. Robertson, "Infrared Reflectance Properties of Aircraft Paints," *IRIS Targets, Backgrounds and Discrimination* (1985).
8. C. Acquista and R. Rosenwald, "Multiple Reflections in Synthetic Scenes," *Proceedings of the Fifth Annual Ground Target Modeling & Validation Conference*, Houghton, MI (1994).